Modelling and analysis of the Nîmes arena and the Arles aqueduct subjected to a seismic loading, using the Non-Smooth Contact Dynamics method

Ali Rafiee, Marc Vinches, Claude Bohatier

Modelling and analysis of the Nîmes arena and the Arles aqueduct subjected to a seismic loading, using the Non-Smooth Contact Dynamics method

Ali Rafiee [a,1], Marc Vinches [a,*], Claude Bohatier [b,2]

[a] Alès School of Mines, 6 av. de Clavières 30319, Alès cedex, France
[b] LMGC-UMR 5508, Université Montpellier II, CC 048 Place Eugène Bataillon, 34095 Montpellier cedex 5, France

A B S T R A C T

Large stone course structures such as Roman amphitheatres or aqueducts can be modelled as collections of rigid or deformable discrete elements. The "Non-Smooth Contact Dynamics" (NSCD) computational method, on which the LMGC90® code used in this paper is based, is well suited to the dynamic simulation of the behaviour of such large collections of bodies with complex three-dimensional geometries. The obtained results for the simulation of the dynamic excitation for two examples of real antique structures, "Nîmes arena" and "Arles aqueduct" in France, are presented. The mechanical behaviour of the numerical models is then examined and, where possible, compared to the present state of the two-millennia-old structures.

Keywords:
Masonry modelling
Seismic loading
Non-Smooth Contact Dynamics method
Nîmes arena
Arles aqueduct

1. Introduction

The modelling of the structural behaviour of a historic construction may appear as a standard task in a basic mechanical system. A historic building, even from a mechanical point of view, appears as a complex system. Over the last twenty years, constitutive models and calculation techniques that enable realistic description of the structural behaviour of masonry structures have become available [1–11].

Masonry structures are made of stone blocks, often bonded by mortar joints. When the global behaviour of an entire structure was investigated, it has often been necessary to assume a properly homogenised material and perform the analysis using the finite element method. According to Giordano et al. [12] when a single structural element was being studied, the actual distribution of blocks and joints was rarely accounted for.

In this study, a general procedure for assessing the stability of historic masonry is proposed using the LMGC90® code with 3D rigid element modelling. In addition, 2D deformable investigations are performed for several chosen sections. This approach is applied to the study of the Arles aqueduct and the Nîmes arena (France). The structural characteristics and the stability during an earthquake vibration of these two monuments are studied. The main aim of the study is to determine the weakness zones of this type of structure during seismic events. In special cases, when a body in the model is subjected to a high pressure, it can be studied at a local scale by a 3D deformable model. The loads at its boundaries are provided by the global model. In the LMGC90 code there is the possibility to model propagation of cracks within masonry units using the frictional Cohesive Zone Model (CZM) [13]. Concerning the possible failure of the masonry elements, and the dilatancy of the masonry considered as the spherical part of the volumic dilation of a specially designed strain tensor in rigid element assemblies, details can be found in [7,14].

The results obtained by such an analysis can be used to reinforce the historic monuments, or to perform more accurate monitoring at the locations revealed as the most vulnerable. The deterioration of the friction coefficient might depend on the relative displacements of blocks. However, it seems that a local sophistication when the global behaviour of the structure is analysed, seems useless. The determination of a coefficient of friction, changing with the displacement, would have to be made in laboratory experiments, and supposed to be representative of a general behaviour in the monument. This later hypothesis is strong enough, and the refinement interest seems, to the authors, irrelevant, for this type of study, where the global behaviour of the structure is the main objective of the work. There is a possibility to insert a static and a dynamic coefficient of friction in the friction

* Corresponding author. Tel.: +33 4 66 78 56 67; fax: +33 4 66 78 53 65.
E-mail addresses: ali.rafiee@ema.fr (A. Rafiee), marc.vinches@ema.fr (M. Vinches), bohatier@lmgc.univ-montp2.fr (C. Bohatier).

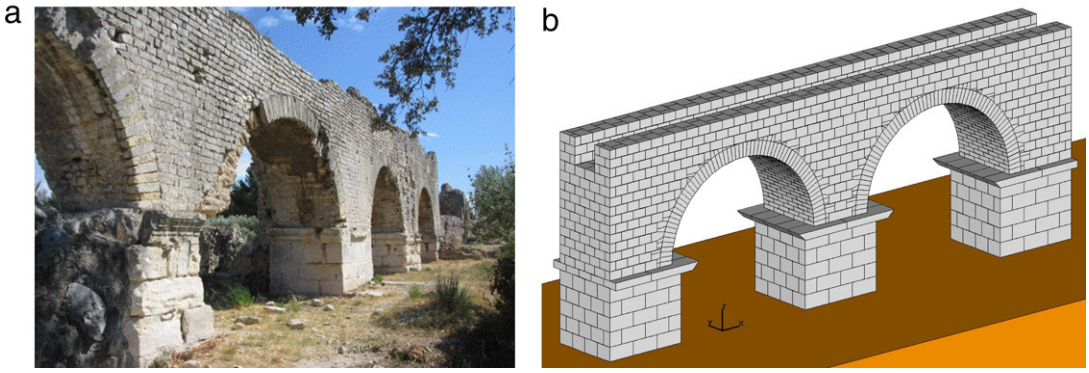

Fig. 1. Arles aqueduct (a) arches showing large stone course pillars, (b) 3D model generated in AutoCAD environment for two arches with 2974 discrete blocks and with an arch span of 4.8 m.

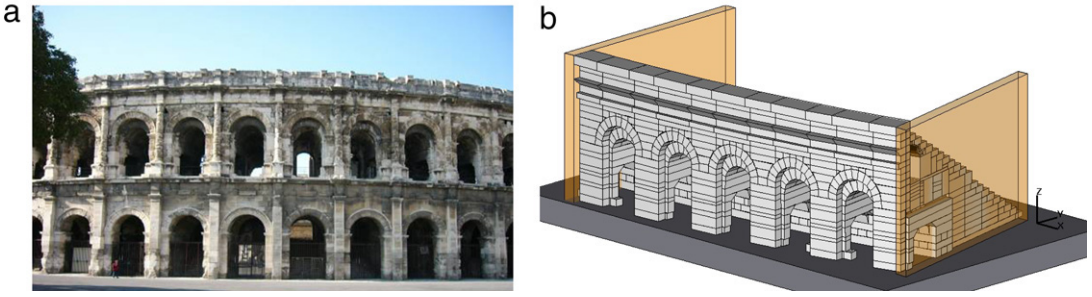

Fig. 2. Nîmes arena, (a) Exterior view (b) 3D model generated with AutoCAD software including 2670 blocks for five arches on the first floor.

law, this seems to be a sophisticated enough model. In this study, the NSCD method incorporated in the LMGC90® code is used to perform the mechanical modelling. A brief explanation of the NSCD method is provided in the Appendix.

A short presentation of the two historic structures and of the characteristics of their numerical models follows. The results obtained for the structural analysis and after seismic vibrations are given for both constructions. Finally, a comparison is made between the behaviour of the model and the present state of the monuments. The studied structures are both listed buildings, and are protected by the French law on built heritage. No retrofitting is envisaged by the state agency in charge of the two buildings.

2. Case studies

2.1. Arles aqueduct

During the second century A.D., the complete rebuilding of an aqueduct bridge at the Vallon des Arcs site, near Fontvielle (France), can be explained by the necessity to supply the Roman colony of Arles with water [15]. The site reveals the presence of two parallel 325 m long aqueducts.

The western bridge was used by the aqueduct leading to Arles; the waters were gathered on the north side of the Alpilles. The second bridge supported a conduit leading to the Barbegal mills; the waters were collected on the south side of the Alpilles. Built on the south side of the limestone rock mass, this exceptional building housed 16 stone mills able to run simultaneously. It was the biggest known milling complex of this type in the Roman world.

The conduit of the Arles aqueduct was first laid on a 49 m long retaining wall, then on a 249 m long bridge. The arch stones were almost 2.1 m long and the aqueduct consisted of 36 piers. The average width of the aqueduct is 2 m, Fig. 1.

The foundations, the piles and the arches, on the north side, are in large dry assembled stone blocks (without mortar). The other arches and the conduit are in masonry (stone blocks with mortar). The outside walls of the arches and of the conduit were made of small stone parallelepiped blocks. The sealing of the conduit is ensured by a 0.25 m thick layer of concrete and a 0.05 m mortar coating. The large blocks used in the aqueduct's construction are shelly yellow limestone, probably extracted from the stone quarry located under the present village of Fontvieille. The mechanical and physical properties of the materials used in the aqueducts were mainly obtained, in different academic laboratories, in the framework of D. Raffard's doctorate studies [16].

The assumption of a ruin accelerated by consecutive movements of the ground, due to the construction of the parallel aqueduct, is currently one of the most plausible. The addition of the stone mass, brought near the first Arles aqueduct to build the Barbegal aqueduct, could involve a compression of the layers composing the foundations, up to the limit of their supporting capacity. A seismic phenomenon should not be excluded either, although its evidence on the site is nearly impossible to establish due to the quasi-disappearance of the first bridge. Concerning the collapse of the Barbegal aqueduct, and of the second Arles aqueduct, a seismic phenomenon is considered a possible cause [15].

2.2. Nîmes arena

The amphitheatre, more commonly called an arena, was built at the time of the Roman emperors for public entertainment. The Nîmes arena is one of most beautiful and best preserved Roman arenas.

The amphitheatre is an ellipse. Its east–west axis is slightly more than 133.3 m long and its north–south axis is 101.4 m long. The width of the constructions, from the outside wall of the arena, to the inside the ellipse, is 33.5 m. The height of the amphitheatre, from the external base up to the crowning level of the attic, is approximately 21.3 m. Four doors, north, east, south, and west facing, give access to the interior of the arena (Fig. 2a) [17].

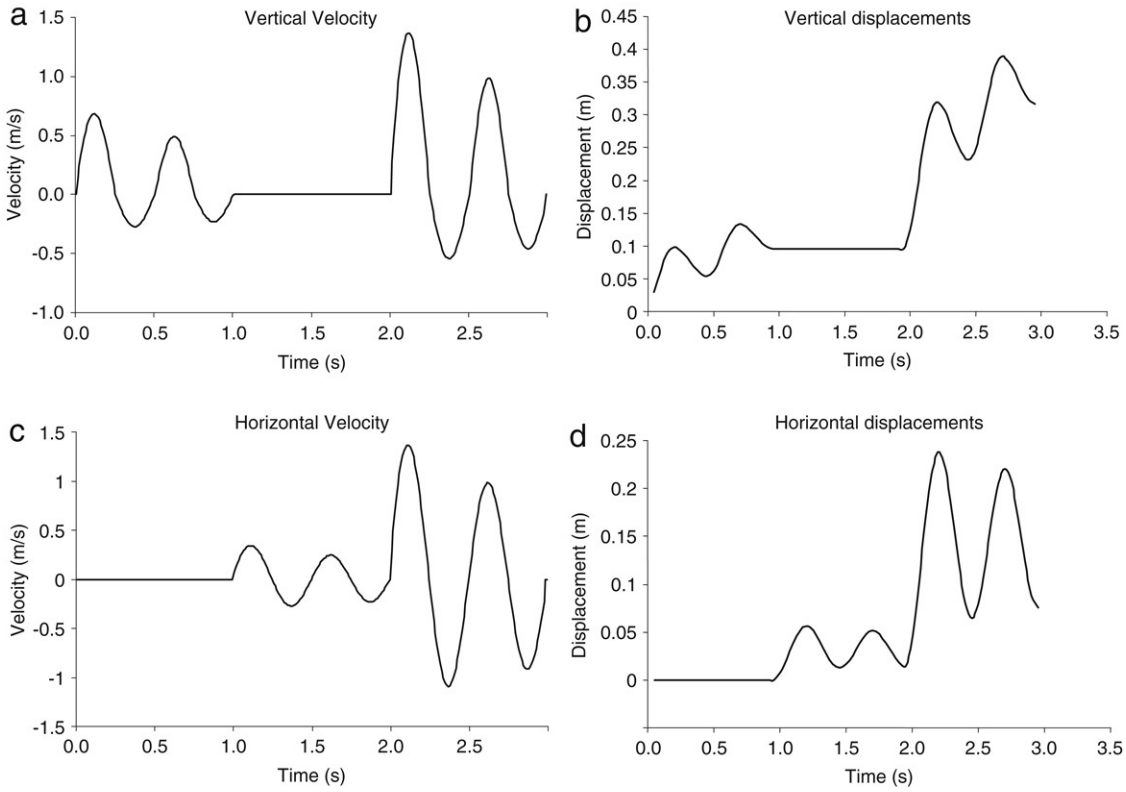

Fig. 3. Input velocity versus time, in m/s, applied to the base element, and corresponding induced displacements versus time, in metre: (a) vertical velocity, (b) vertical displacements, (c) horizontal velocity, and (d) horizontal displacements.

The external wall is made of two arches, one on top of the other. It is surmounted by an attic and is divided into sixty radiant spans which form the circular divisions of the arena. The height of the ground floor arches is approximately 6.3 m while that of the first floor is 6.5 m. All of them have an opening of approximately 6 m [17].

The knowledge about the stones used in the arena is of primary importance, for restoration purposes. The stones employed in the arena are mainly Barutel stone extracted from a stone quarry situated near the city of Nîmes. The stones are a compact fine grain limestone.

The 3D model of the arena is generated from the data measured *in situ* (Fig. 2b) [18]. The model, as was the case for Arles aqueduct model, is drawn using AutoCAD software. Then, using a specific program developed in this environment in LISP and Visual Basic, the model file is converted into a standard text format file to be used in the LMGC90 code. The model of the arena, in which we have 2670 discrete blocks, consists only of the five arches on the first floor, including the attic wall and gallery.

3. Seismic simulation

France is a country of moderate to low seismicity with a ten-century record of historical seismicity that shows approximately five major destructive earthquakes [19]. Although the source parameters of these earthquakes are still not precisely known, their magnitudes are roughly estimated to be no higher than about $M = 6$ and their destructive effects are commonly attributed to poor building quality. Epicentres of French historical and instrumental seismicity are located mainly in mountain chains and depressions (Pyrenees, Alps, Jura and Rhine Graben) and in the old Palaeozoic massifs (Massif central, Brittany, and Ardennes).

Paleoseismic data collected on French fault zones confirm that seismic events with nearly $Mw = 7$ occurred in France [19–22]. The seismicity of southern France probably results from the convergence between Africa and Europe which proceeds at a rate of approximately 0.8 cm/year at the Provence longitude [23]. The most interesting data were obtained at three localities in Provence (Nîmes fault), Aquitaine Basin (Meilhan) and southernmost Alps (Argentera fault). The NE-SW striking Nîmes fault extends over 100 km from north-western Provence to the Gulf of Lion. The two masonry structures in this study are located in the seismicity zone of this active fault.

In this study, we intend to investigate the effect of a real seism on these two historic masonry monuments. For this purpose, two types of seismic excitation are used. First, in order to better understand a seismic excitation effect on a masonry structure, an artificial vibration is employed. In fact, hypothetical horizontal and vertical loadings based on a sinusoidal vibration of 2 Hz are applied to simulate a seismic oscillation. This vibration system is used as a velocity function at the foundation level of each model. The supporting element in the model is assigned continuous velocities, in three dimensions, as a function of time. In this way, the masonry models are based on a supporting element that acts as a shaking table, oscillating with vibrations in three directions. The graphs of the vibration velocities and the displacements induced by these input velocities for horizontal and vertical components, used for both models, are shown in Fig. 3. It should be noted that the displacement values for the base element are obtained through post-processing data recorded during computation.

As can be seen in these graphs, three distinct phases were chosen for the seismic vibrations. This was done to study the dynamic behaviour of the concerned structures separately, for vertical and horizontal displacements, then for combined displacements. In this way, the direction of vibration for which the structure is more vulnerable can be distinguished. A real seism would present similar vibration characteristics. The general behaviour of the structure for an earthquake of the same scale could then be predicted.

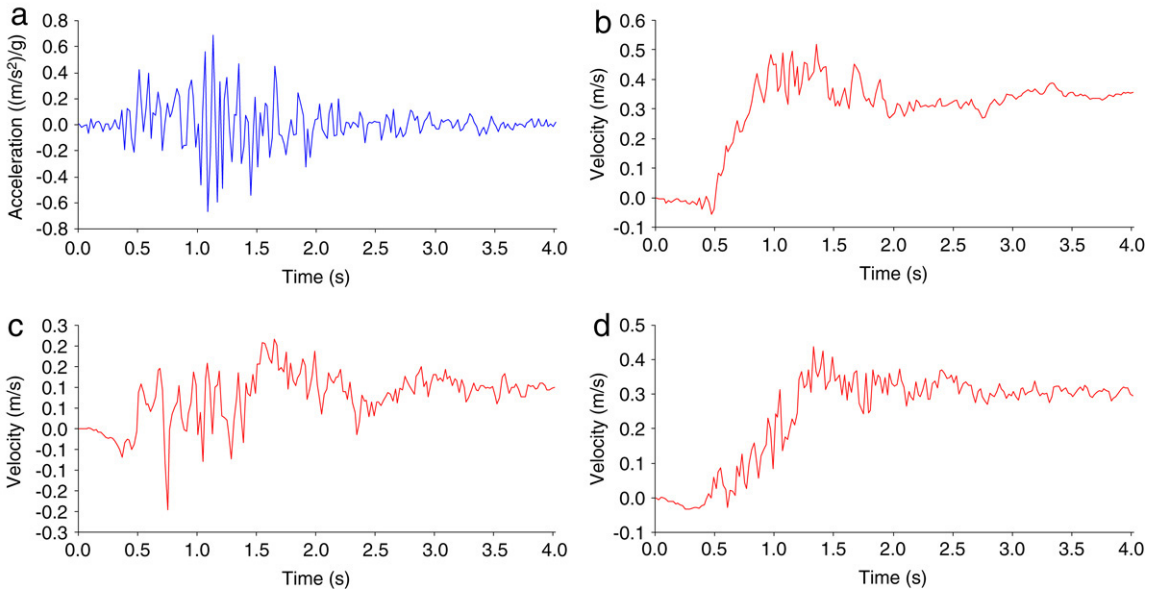

Fig. 4. (a) Accelerogram, vertical ground acceleration in g (9.81 m/s2); (b) vertical ground velocity (m/s); (c) horizontal velocity in the *X* direction; (d) horizontal velocity in the *Y* direction.

Table 1
Mechanical, physical and calculation parameters used in the models

Models	Parameters				
	Density (kg/m^3)	Friction coefficient	Young modulus (GPa)	Poisson ratio	Time step (s)
2D rigid model	2000	0.7	–	–	5e−3
2D deformable model	2000	0.7	25	0.25	1e−3
3D rigid model	2000	0.7	–	–	1e−3

Since the aim of the paper is the study of the behaviour of masonry structure and its failure modes in the event of seismic motion, the model of Arles aqueduct is subjected to a real seismic excitation. Part of the accelerogram of a recorded earthquake with a maximum vertical acceleration of 7 m/s^{-2} and with a four second duration is used in three directions (Zanjiran earthquake, Iran, June 20th 1994, an earthquake with a magnitude of about 6.1-mb) [24]. The graphs in Fig. 4 illustrate the input velocities used in the three directions applied to the supporting element of the model.

The seismic analysis is performed for both models in two and three dimensions. Each model will be studied with rigid elements in three- dimensional simulations, and with deformable and rigid elements in two dimensions.

3.1. *Analysis results for the Arles aqueduct*

Static and dynamic analyses are carried out on the 3D and 2D models of the Arles aqueduct using the LMGC90 code. The masonry structures are modelled as a collection of discrete blocks of approximately the real size, as observed *in situ* (Fig. 1) [14,15]. A 2D section of the 3D model is used for 2D modelling. In the first step, a 2D rigid model of the aqueduct with five arches is used for both real (Fig. 5a) and artificial (Fig. 5b) seismic excitation. It should be noted that the aqueduct model is not fixed laterally, because the actual *in situ* structure is not a continuous structure. In order to take into account the real state of the structure in both 2D and 3D models, the aqueduct is considered with no restriction for lateral displacement.

However, in order to investigate the effect of the lateral displacement condition, the model with five connected arches is subjected to a seismic excitation. For this model, the interaction law between blocks is considered to follow the Mohr–Coulomb law with a friction coefficient equal to 0.7, and the density of the blocks is 2000 kg/m^3 (Table 1). Fig. 5a shows the results obtained for this model with seismic vibration shown in Fig. 4. It should be noticed that in all 2D models with real seismic excitation, the horizontal vibration applied to the models is the vibration in the *X* direction illustrated in Fig. 4c. As can be observed in Fig. 5a, all five arches present approximately the same failure mode. Two points of weakness can be distinguished for each arch depending on the arch position, but with the same location. Fig. 5c and d illustrate a close-up view of the vertical displacements (in metre) for the central arch for both the real seismic excitation and the sinusoidal loading, respectively. The evolution of the number of sliding contacts during the seismic excitation is presented in Fig. 5e. A sharp increase in the number of sliding contacts is seen just after the first half second, which is directly related to the dramatic change in the horizontal displacement (Fig. 4c).

As previously explained, the 2D rigid model of the Arles aqueduct for five arches (Fig. 5) showed nearly the same failure mode, consequently 2D deformable analysis was carried out for only two arches. The model is meshed in triangular elements using the Gmsh software (Fig. 6). This model contains 588 separately meshed blocks and the Mohr–Coulomb law, with a 0.7 friction coefficient, applies for contact points between blocks. In all deformable models, the Young modulus is 25 GPa, Poisson's ratio 0.25 and density 2000 kg/m^3. Fig. 6 shows the result obtained for the vertical displacements using the three-second-long sinusoidal vibrations (Fig. 3). As can be seen in this figure, two more sensitive zones at which the collapse of the structure begins can be distinguished for each arch.

By continuing the seismic vibration, it is observed that the structure is more vulnerable to horizontal vibration, particularly in the third phase of vibration: simultaneous strong horizontal and

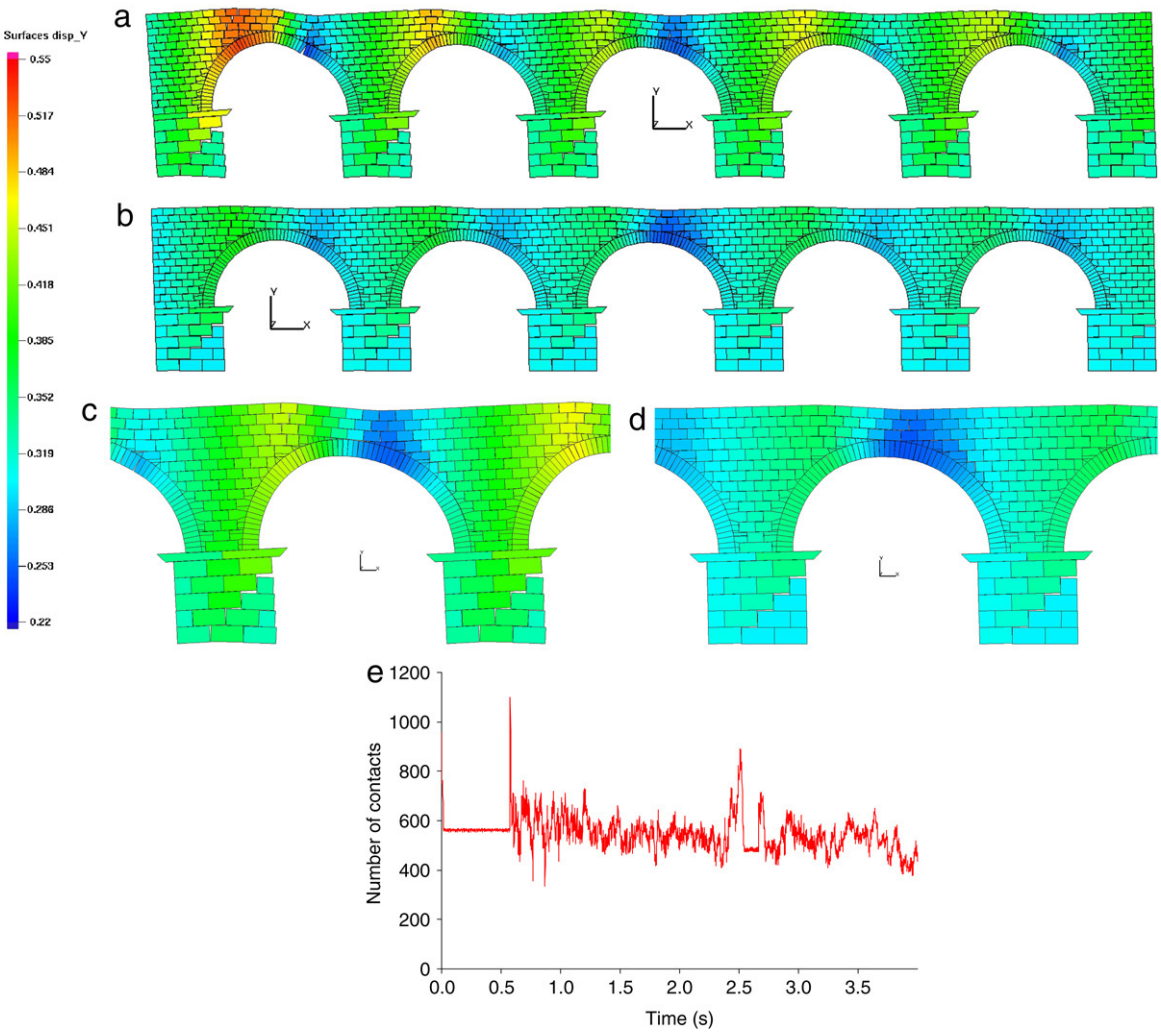

Fig. 5. Vertical displacements (in metre) for 5 consecutive arches of the Arles aqueduct, in a 2D rigid model, (a) real seismic vibration (Fig. 4), (b) artificial sinusoidal vibration (Fig. 3) (c) close-up view from the central arch for real seismic excitation, (d) close-up view from the central arch for sinusoidal seismic excitation, (e) evolution of the number of sliding contacts during four seconds of the real seismic vibration.

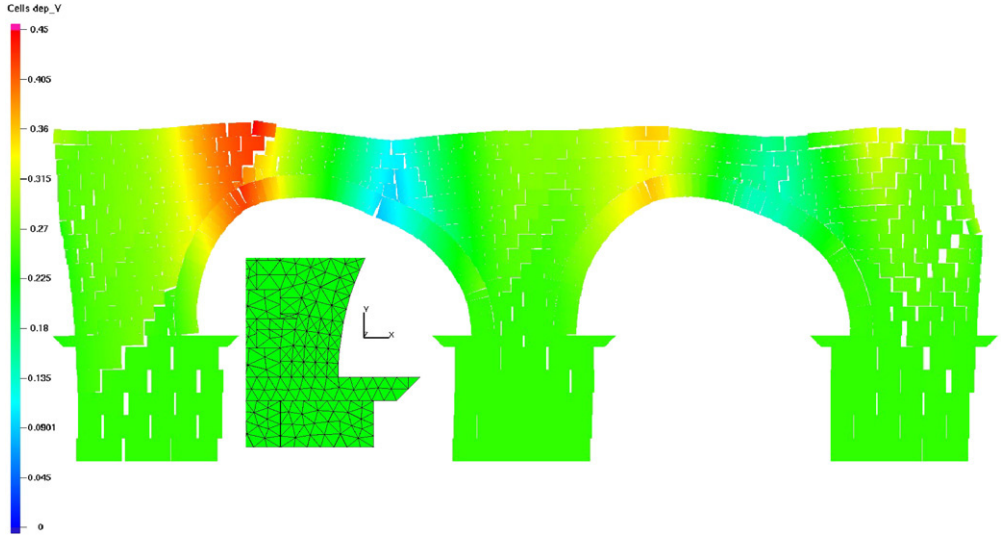

Fig. 6. 2D deformable model displacements in the vertical direction, after three seconds of sinusoidal vibration (in metre).

vertical vibrations. The relative displacements of the blocks are clearly seen in Fig. 4. The structure starts to lose its continuity, and begins to collapse.

In order to better understand the effect of a seismic vibration on such a structure, the 3D model with real block dimensions is studied, see Fig. 1. For static analysis, the 3D model is studied

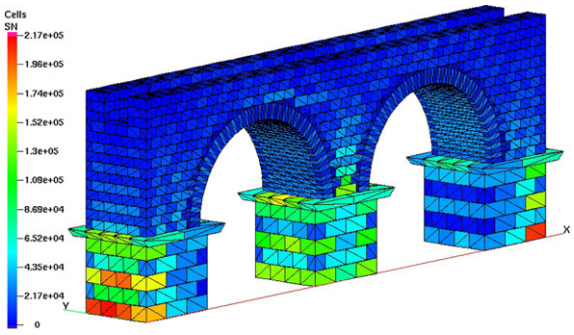

Fig. 7. 3D rigid model, distribution of the vertical forces on each block (in N).

under its weight and Fig. 7 shows the distribution of vertical forces over the model. In fact, this analysis can be used to distinguish the blocks supporting a high vertical force. In this model, the rigid blocks are used by considering the same mechanical parameters, as indicated in Table 1, and a friction coefficient of 0.7. Contrary to the continuous method, in this model we can observe, block by block, the vertical forces induced from upper blocks. These results can be used for a local reinforcement or repairs of the structure. As previously mentioned, there is a possibility to determine for each block, a volumic stress threshold, leading to a local examination of the most loaded blocks. A 3D deformable modelling of such a block is then possible, taking the local forces acting on it as boundary and loading conditions [17].

For the 3D rigid model, the same vibration systems are employed to investigate the seismic behaviour of the structure. In the case of real seismic excitation, the obtained results (Fig. 8) show that block detachments occur locally in the exterior part of the arches. This is clearly observed in Fig. 8(b). It should be mentioned that this kind of block detachment is also visible on the *in situ* structure (Fig. 1a). Another interesting result of this 3D model is that larger lateral displacements occur on the level of the pillars in comparison with the displacements of the blocks in the arches. Fig. 8c illustrates the upper view of the structure after four seconds. Joint opening is more visible over the pillar.

The evolution of the number of sliding contacts during this four second vibration for the 3D model is presented in Fig. 9a. There is a sharp increase in the number of sliding contacts just in the first half second, which is caused by simultaneous changes in all three components of the seismic vibrations, and especially in the vertical one (Fig. 4). After the first second, the number of contacts remains without high fluctuation, because of the smoothness observed in the seismic oscillations, however this number remains about a fourth of the all active contacts. The ascending graph presented in Fig. 9b shows the total dissipated energy during the vibration by friction and shock.

In the second phase of the seismic vibration, the aqueduct structure is subjected to an artificial seismic excitation presented in Fig. 3 which has three distinct phases. In the first phase of the vibration that is dedicated only to the vertical one, the model does not show a large instability, but when the horizontal vibration arrives, the structure begins to lose its stability. The results

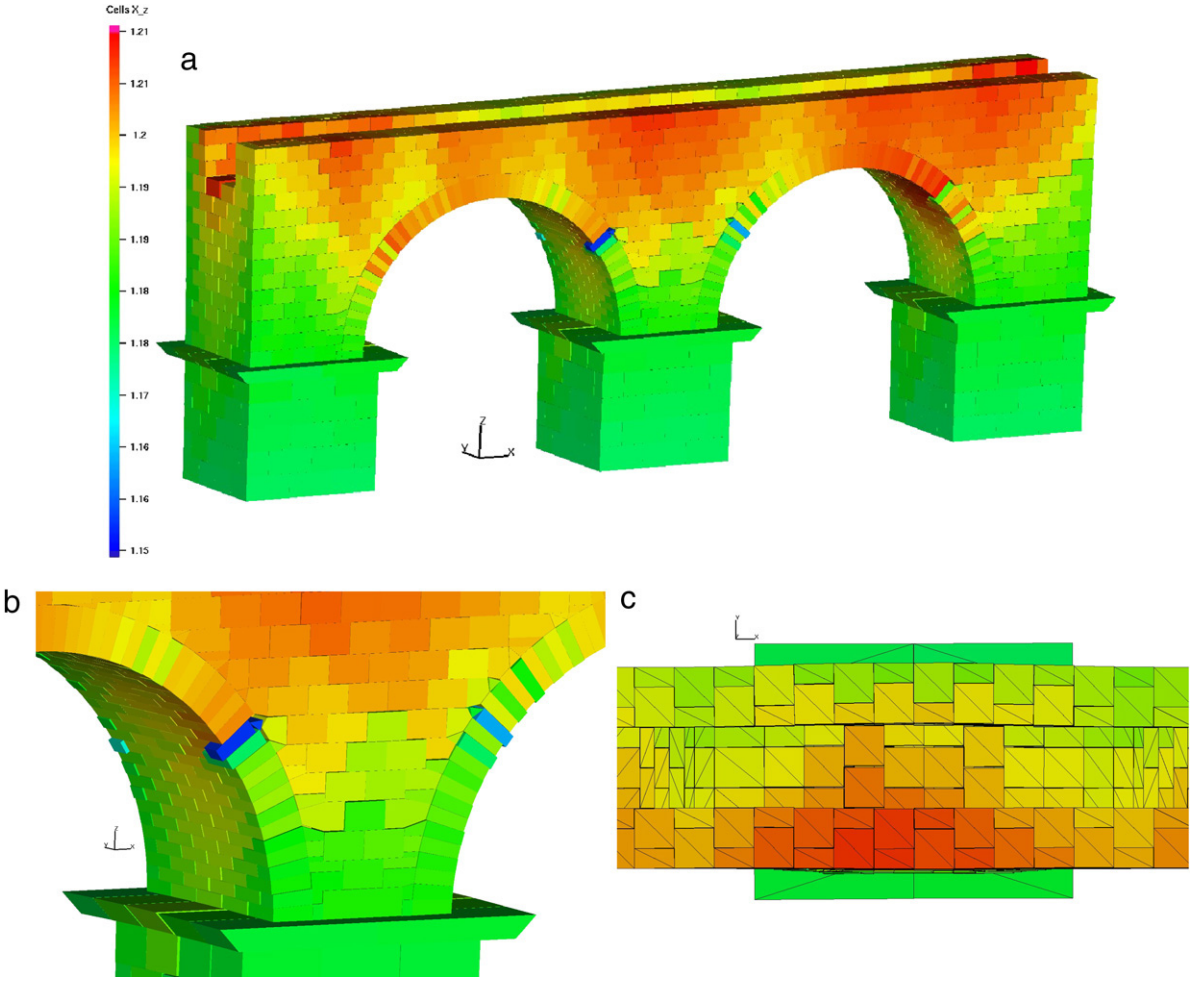

Fig. 8. 3D rigid model, vertical displacements (in metre) resulting from four seconds duration real seismic vibrations (a) after four seconds, (b) close-up view on the arch structure (c) view from above.

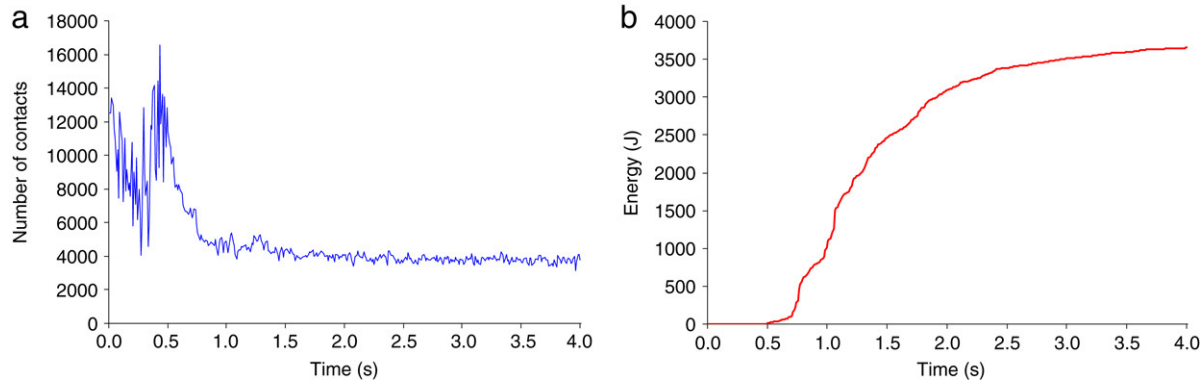

Fig. 9. (a) Evolution of the number of sliding contacts during four second real seismic vibration (Fig. 4) in the 3D rigid model for the Arles aqueduct, (b) dissipated energy during the seismic excitation.

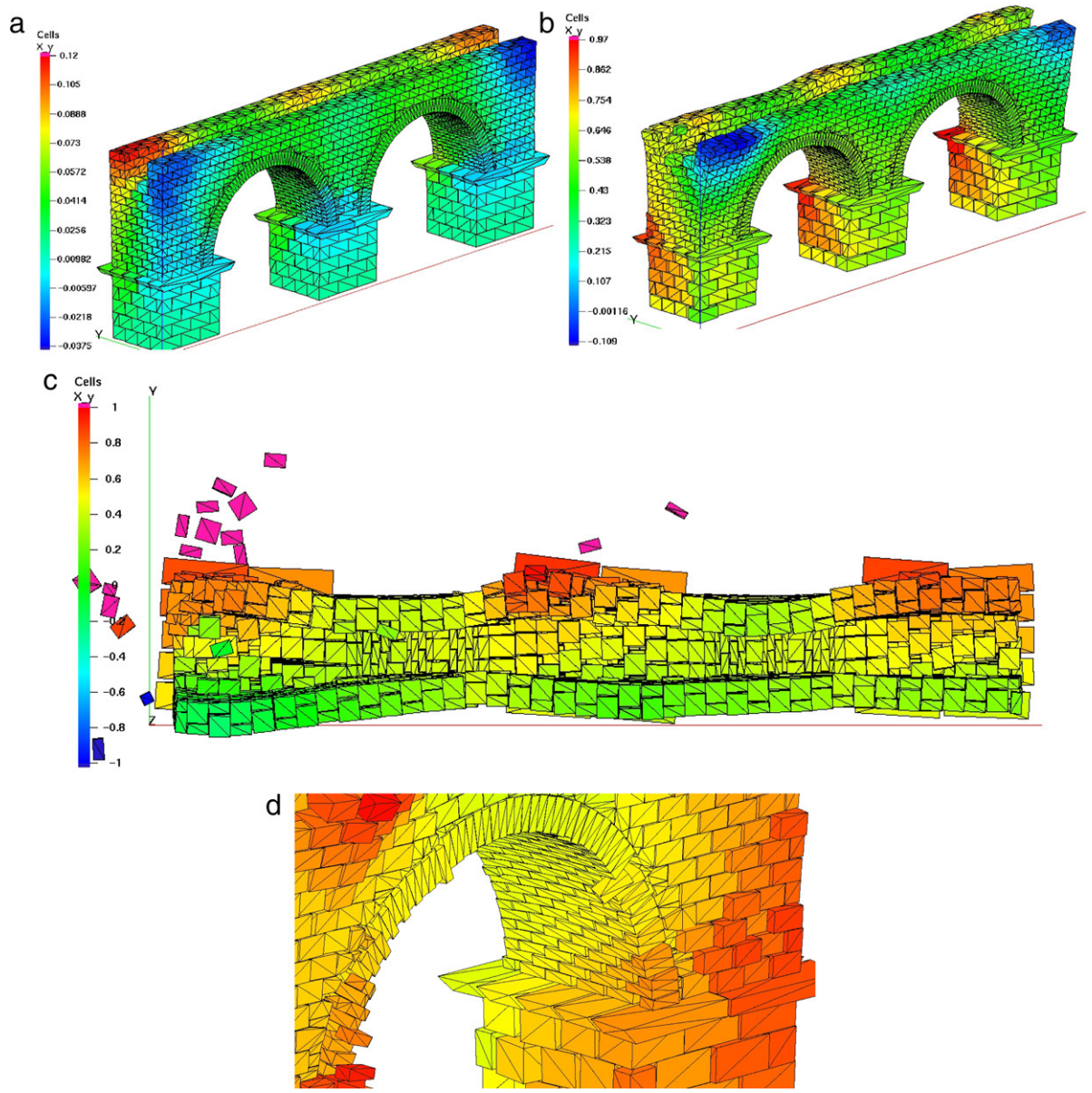

Fig. 10. 3D rigid model, displacement (in metre) in the *Y* direction resulting from three seconds duration seismic vibrations (a) after two seconds (b) after three seconds, (c) view from above at the 50th second, (d) close-up view on the arch structure.

obtained for two phases of the vibration are illustrated in Fig. 10. As can be observed in Fig. 10a, which shows the displacements in the *Y* direction, the structure remains stable for the first two seconds with a maximum 0.12 m lateral displacement. However

by continuing the vibration, in Fig. 10b, it is seen that at the end of the third second of the vibration, the structure loses its stability and begins to collapse. As in the 2D model, during the calculation, it can be noticed that the structure has a weak resistance against horizontal vibrations, especially if it is accompanied by vertical vibration. This is observed in Fig. 10b. It should be remarked that in the 3D models, a triangulation is performed for the discretisation of the surfaces of the blocks in order to facilitate the contact detection procedure. The diagonal lines on the surfaces of the blocks merely indicate this triangular division.

The calculation after the first three seconds is continued without any vibrations, in order to observe the final state of the structure. Fig. 10c shows the state of the aqueduct after the 10th second of the calculation. This figure displays a view from above of the structure and reveals clearly high lateral displacements which occurred at the level of the pillars, as observed *in situ*. The close-up image (Fig. 10d) from a lateral view, shows the arch structure with block detachments from its exterior part. By comparing the results obtained with the seismic simulations and the present condition of the structure, it seems possible that an earthquake could produce this type of result.

3.2. Results analysis for the Nîmes arena

As in the case of the Arles aqueduct, the same procedure is used for the masonry structure of the Nîmes arena. Firstly, considering the geometrical complexity of this structure, a 2D section is studied for static analysis. It should be noted that the model of the Nîmes arena is investigated only with artificial seismic vibrations (Fig. 3).

The authors are fully aware of the importance of the out of plane stresses and forces, due to the elliptical structure of the monument. In Fig. 11a, the result of the static analysis on the 2D deformable model is shown in terms of horizontal displacements caused by the weight of the blocks. Because of material similarities between the two monuments, the same mechanical parameters as those used for the Arles aqueduct are used for this model (Table 1). As can be observed in this figure, a maximum 1 mm lateral displacement is seen in the 2D section. For the boundary condition of the model, no restriction for lateral displacement is considered in the 2D model, but in the 3D model, the structure is restricted laterally by two planes connected to the supporting plane: these three planes move together. In this way, the rest of the arena is replaced by two lateral planes (Fig. 2b).

The 2D section extracted from the 3D model was subjected to an artificial seismic vibration (Fig. 3) whose characteristics are equal to those employed for the Arles aqueduct case. Fig. 11b illustrates the results obtained for the vibration after three seconds. In this figure, one can see that the upper arch is the most vulnerable part of the structure. In fact, horizontal forces produced in this arch push the supporting wall toward the outside of the arena. As a result, this is where the structure begins to collapse.

Considering the large size of the arena, its quasi-periodic structure and the required calculation time, the 3D modelling of the Nîmes arena is performed on five arches of its first floor, Fig. 2. Of course, it should be mentioned that all the sizes and shapes of blocks in this model were measured *in situ*, to get a geometrical model which is as representative as possible [16,17].

The result obtained for the distribution of the vertical forces induced by the upper blocks is illustrated in Fig. 12. In this way, one can identify the blocks supporting more vertical loads. Dynamic analysis is also carried out for the 3D rigid model of the arena and these results are shown in Fig. 13.

In order to confirm the result illustrated for a 2D deformable modelling in Fig. 11, the results obtained in the 3D model for a vertical displacement are shown in Fig. 13a. As can be observed, high displacements occur at the level of the upper arch for the first

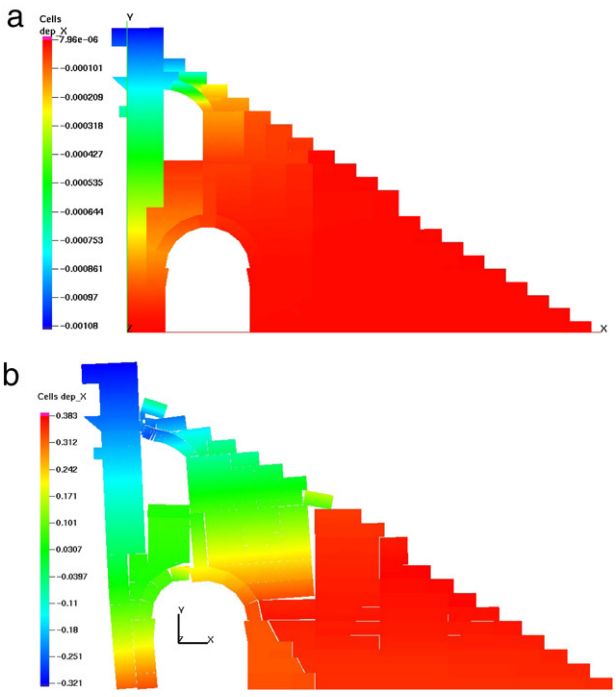

Fig. 11. 2D deformable model of the Nîmes arena, displacements (in metre) in the horizontal direction, (a) subjected to gravity (b) after two seconds of seismic vibrations.

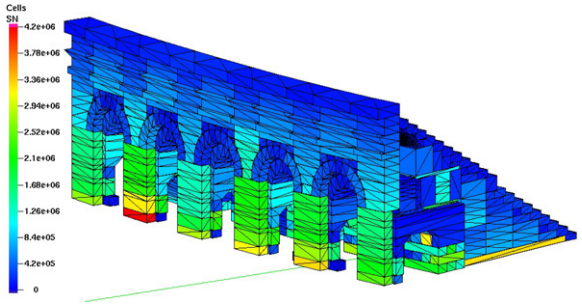

Fig. 12. 3D rigid block model of the Nîmes arena, distribution of vertical forces on each block (in N).

two seconds of vibration. This is similar to the state observed for the 2D model. As a result, this arch should be considered as a weak point for the arena, so more monitoring could be performed on it. Interestingly, it can be pointed out that this part of the building is now destroyed for most of the perimeter of the present monument.

In Fig. 13b, one can see the results obtained for the horizontal displacements in the *Y* direction after the first two seconds of vibration. The same behaviour is seen for the 3D model as anticipated from the 2D model, and the outside wall begins to detach itself from the whole structure, probably under horizontal forces gathered in the upper arch. Consequently, by continuing the vibration application, it can be observed that the total detachment occurs at this point (Fig. 13c).

4. Conclusion

In this paper, two historic Roman masonry structures are analysed to assess their structural and seismic vulnerability. Their behaviour is investigated in a real three-dimensional model. For this purpose, the LMGC90 code is used, due to its ability to compute the interaction of a large number of bodies, based on the NSCD method. 2D deformable and 3D rigid models are built for these two

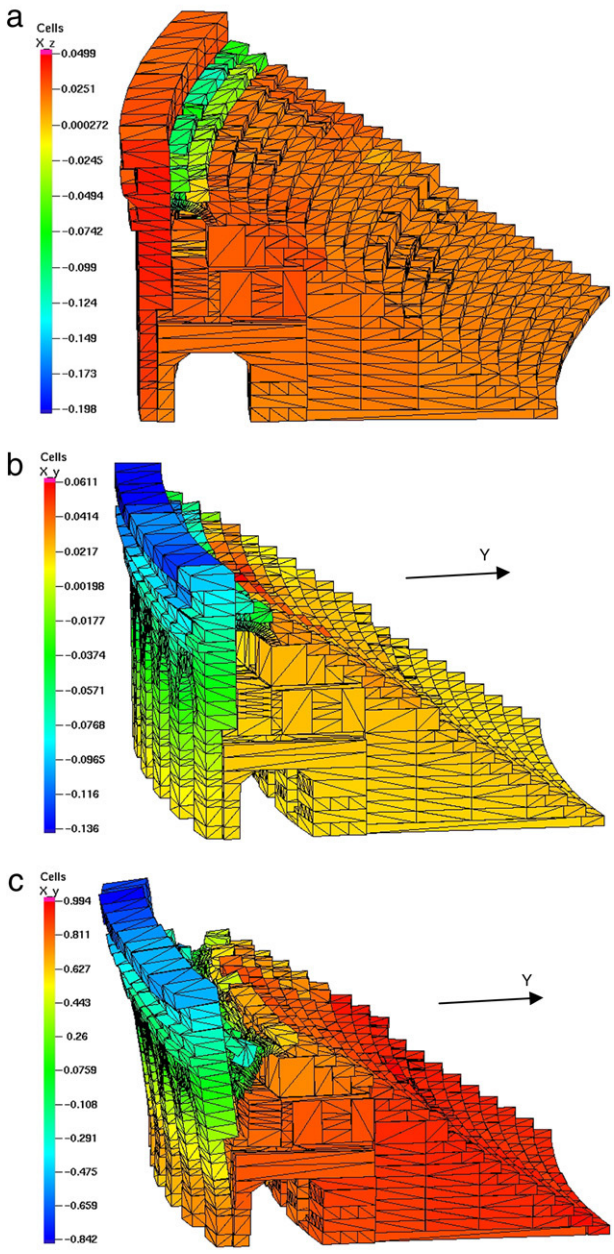

Fig. 13. 3D rigid block models of the Nîmes arena, displacements, in metre, produced by seismic vibrations (Fig. 3), (a) vertical displacement after two seconds, (b) displacement in the *Y* direction after two seconds, and (c) displacement in the *Y* direction after three seconds.

historic monuments. The behaviour of these structures, located in a seismic zone in France, is studied during a real seismic excitation and an artificial simplified one.

The geometry of the models corresponds to the geometry of the real structure, based on *in situ* measurements. The largest possible models are created to better understand the influence of a seism mechanism within the structures. The procedure chosen for simulating the seismic vibration is assumed to be comparable to a real earthquake, producing vibrations in three dimensions.

The results for the vertical force distribution from the static numerical analysis (the structure is subjected to its own weight) give valuable hints for the monitoring of the structure, and allow a realistic determination of the most loaded blocks. The global behaviour of the structures is investigated in this study. Parameters such as exterior and interior forces or shock exerted by the neighbour blocks on each block, during each time step of the calculation, enable us to perform local detailed analyses. The most loaded blocks are of particular interest.

The numerical results obtained using LMGC90 for the study of the mechanical behaviour of the Arles aqueduct, when subjected to a seismic vibration, correspond to its present condition. These results are consistent with archaeologists' hypotheses and seismologists' knowledge. Considering the great historical value of monuments such as this aqueduct, similar studies could be useful to identify the vulnerable points of structures subjected to earthquake vibrations, in order to produce and compare designs to reinforce them. In other words, this study has highlighted that numerical analysis, at this level of accurate geometrical description, can improve the knowledge of the structural behaviour of masonry structures. In addition, numerical modelling can play an important role in the process of structural restoration and reinforcement of antique masonry, particularly in areas with high seismic risks.

The results obtained for the model of the arena in Nîmes, subjected to an artificial earthquake vibration, showed the high vulnerability of this structure, especially at the upper level of the outside wall.

Appendix. The NSCD method

A.1. Parameterisation and equation of dynamics

In computational mechanics, among well-suited approaches for the rigid body dynamics with contact, friction and impact, there are two opposite approaches: compliant versus unilateral contact model and event-driven versus time-stepping schemes. In the context of granular materials, where large collections of bodies are encountered, Cundall [25,26] was the first to propose a numerical tool, based on an Euler scheme, where contacts are governed by a compliant model. With a very different approach, Moreau [27–32] and Jean [33–35] exposed a numerical treatment of rigid and deformable body collections with unilateral contact, Coulomb's dry friction and impact, in the framework of the Non-Smooth Mechanics and Convex Analysis. This framework yields a time-stepping scheme (without explicit event-handling) where velocities and impulses are the primary variables.

This section aims at representing the basic equations of the Non-Smooth Contact Dynamics method (NSCD). The formulation of the NSCD method relies on a special formulation of the equation of motion. The term "non-smooth" refers firstly to the mathematical and mechanical background allowing us to deal with some extended kinds of laws. For the non-smoothness in time, the occurrence of velocity jumps is a well known feature of the second order dynamics with unilateral constraints on the position, even with continuous media.

Additionally, the contact forces between two bodies are bound by the law of action and reaction. The calculation of contact forces in the NSCD method is performed in two steps. First the result of the interaction of the antagonist body B_a on the candidate body B_c can be considered equal to the force r_α acting at the contact point of these two bodies. At the contact point, we can define a local frame composed of three vectors (in a 3D model) including a normal vector n_α pointing from B_a to B_c and two tangential vectors s_α and t_α, which define the tangential space by respecting this convention $s_\alpha \times t_\alpha = n_\alpha$. On the other hand, we denote g_α the gap distance between bodies along the normal direction. This value will be negative if there is interpenetration between the bodies [27,36–38].

In the second step, one defines a linear mapping H_α that relates the local forces to the global force by the following equation:

$$R_\alpha = H_\alpha(q) r_\alpha \tag{1}$$

where $H_\alpha(q)$ is a mapping which contains the local information about contactors. Finally the global contact forces can be obtained by the relation

$$R = \sum_\alpha R_\alpha. \tag{2}$$

The same procedure is employed for velocity calculation and the velocity of the bodies can be expressed in the local frame. The relative velocity u_α at the contact point is defined for two bodies in contact by the following equation:

$$u_\alpha = H_\alpha^{\mathrm{T}}(q)\dot{q} \tag{3}$$

where H^{T} is the transpose of H. The relative velocity is decomposed in a normal component represented by $u_{\alpha,n}$ and a tangential component $u_{\alpha,T} = (u_{\alpha,s}, u_{\alpha,t})$.

It should be noted that the derivative of the gap function is equal to

$$t \to g_\alpha(t) \qquad u_\alpha.n\alpha. \tag{4}$$

During the evolution of the model with multi-contact systems, shocks may be expected. As a result, these shocks produce velocity discontinuities and make it impossible to define the acceleration as the usual second time derivative of the configuration parameter. Hence, the equation, of motion will be written as

$$M\mathrm{d}\dot{q} = F(t, q, \dot{q})\mathrm{d}t + \mathrm{d}R \tag{5}$$

where q is the configuration parameter which can represent the discretised displacement or any generalized coordinates of the rigid motion, dt is the Lebesgue measure on R, d$\dot{q}$ is a differential measure denoting the acceleration measure and dR is a non-negative real measure representing forces and impulses. The matrix M in the Eq. (5) is the mass matrix and the vector $F(t, q, \dot{q})$ collects the internal and external discretised forces acting on the system.

A.2. Frictional contact laws

For determining the value of each component R_α, we need additional information about contact forces. These data are primordial to complete Eq. (5) and also to describe the motion of the system in question.

The impenetrability of contact evoked previously means that it is impossible to have two bodies with crossing boundaries in the system. In addition, it is also considered that the contacting bodies are not attracting each other. In other words, the normal component of the reaction force is always positive or equal to zero when the contact vanishes. This contact behaviour is known as the first unilateral constraint or Signorini condition:

$$g \geq 0 \qquad r_n \geq 0 \qquad g.r_n = 0. \tag{6}$$

In the case of cohesive contact, shifting is applied to r_n which represents a cohesive force. This shifting is set to zero if the contact is broken.

The second unilateral constraint, in the case of Coulomb dry friction, can be summarised by the following equations:

$$\begin{cases} \text{if } |\,\|u_t\| = 0, & \|r_t\| \leq \mu r_n \\ \text{if } |\,\|u_t\| \neq 0, & \|r_t\| = \mu r_n, \quad u_t = -kr_t, k \geq 0. \end{cases} \tag{7}$$

The friction force lies in Coulomb's cone ($\|r_t\| \leq \mu r_n$, μ friction coefficient) and if the sliding velocity is different from zero, friction force is opposed to the sliding velocity with magnitude μr_n.

A.3. Numerical scheme for time integration

One of the most interesting features of the time-stepping integration scheme is included in the fact that it does not have to handle explicitly the contact events, contrary to the usual event-driven scheme. When we proceed to a time discretisation on intervals $[t_i, t_{i+1}]$ of length h, our contact problem is solved over the interval in terms of measures of this interval and not in a pointwise way [36]. To achieve this property, the Eq. (5) is integrated on each subdivision, which leads to

$$\begin{cases} M(\dot{q}_{i+1} - \dot{q}_i) = \displaystyle\int_{t_i}^{t_{i+1}} F(t, q, \dot{q})\mathrm{d}t + R_{i+1} \\ q_{i+1} = q_i + \displaystyle\int_{t_i}^{t_{i+1}} \dot{q}(t)\mathrm{d}t \end{cases} \tag{8}$$

where the variable $\dot{q}_{i+1}$ denotes the approximation of the right limit of the velocity at the time t_{i+1}, and $q_{i+1} \approx q(t_{i+1})$. For the contact d$R$, we approximate the measure of the time interval $[t_i, t_{i+1}]$ by dR denoted by

$$\mathrm{d}R([t_i, t_{i+1}]) = \int_{[t_i, t_{i+1})} \mathrm{d}R \cong R_{i+1}. \tag{9}$$

To approximate the two integrals of the system (8), we use a θ-method, which is a first-order scheme using only the configuration parameter and its first derivative. It should be mentioned that a θ-method is an implicit scheme, identical to the Backward Euler's scheme when $\theta = 1$. The stability condition of the scheme implies that θ remains between 0.5 and 1. This approximation leads to the following equation,

$$\begin{cases} \displaystyle\int_{t_i}^{t_{i+1}} F(t, q, \dot{q})\mathrm{d}t = h\theta F(t_{i+1}, q_{i+1}, \dot{q}_{i+1}) \\ \quad + h(1-\theta)F(t_i, q_i, \dot{q}_i) \\ q_{i+1} = q_i + h\theta\dot{q}_{i+1} + h(1-\theta)\dot{q}_i. \end{cases} \tag{10}$$

To complete the discrete form of the dynamical equation, a discretisation of the frictional contact law that is beyond of the scope of this study, must also be performed. A more detailed discussion on the NSCD method can be found in [13,27,31,36–39].

References

[1] Betti M, Vignoli A. Modelling and analysis of a Romanesque church under earthquake loading: Assessment of seismic resistance. Eng Struct 2007; doi:10.1016/j.engstruct.2007.03.027.

[2] Burnett S, Gilbert M, Molyneaux TCK, Beattie G, Hobbs B. The performance of unreinforced masonry walls subjected to low-velocity impacts: Finite element analysis. Int J Impact Eng 2007;34:1433–50.

[3] Cakmak A, Moropoulou A, Mullen CL. Interdisciplinary study of dynamic behavior and earthquake response of Hagia Sophia. Soil Dynam Earthquake Eng 1995;14:125–33.

[4] Carpinteri A, Invernizzi S, Lacidogna G. In situ damage assessment and nonlinear modelling of a historical masonry tower. Engineering Structures 2005;27:387–95.

[5] Chaimoon K, Attard MM. Modeling of unreinforced masonry walls under shear and compression. Engineering Structures 2006; doi:10.1016/j.engstruct.2006.10.019.

[6] Fanning PJ, Boothby TE. Three-dimensional modelling and full-scale testing of stone arch bridges. Comp Struc 2001;79:2645–62.

[7] Chetouane B, Dubois F, Vinches M, Bohatier C. NSCD discrete element method for modeling masonry structures. Internat J Numer Methods Eng 2005;64(1): 65–94. doi:10.1002/nme.1358.

[8] Lemos JV. Numerical issues in the representation of masonry structural dynamics with discrete elements. In: Thematic conference on computational methods in structural dynamics and earthquake engineering. 2007.

[9] Mele E, Luca AD, Giordano A. Modelling and analysis of a basilica under earthquake loading. J Cultural Heritage 2003;4:355–67.

[10] Wua C, Haoa H, Lub Y. Dynamic response and damage analysis of masonry structures and masonry infilled RC frames to blast ground motion. Engineering Structures 2005;27:323–33.

[11] Zucchini A, Lourenço PB. A coupled homogenisation-damage model for masonry cracking. Comp Struc 2004;82:917–29.

[12] Giordano A, Mele E, Luca AD. Modelling of historical masonry structures: Comparison of different approaches through a case study. Engineering Structures 2002;24:1057–69.
[13] Jean M, Acary V, Monerie Y. Non smooth contact dynamics approach of cohesive materials. Philosophical Trans Math, Physical Eng, The Royal Soc, London A 2001;A359(1789):2497–518.
[14] Chetouane B, Bohatier C, Vinches M. Mixed deformable/rigid NSCD discrete element method for the modelling of masonry structures. In: Proceedings of European congress on computational methods in applied sciences and engineering ECCOMAS 2004.
[15] Leveau P. Les moulins de Barbegal, les pont-aqueducs du vallon des Arcs et l'histoire naturelle de la vallée des Baux (Bilan de six ans de fouilles programmées). CRAI. Janvier-mars 1995. p. 115–44.
[16] Raffard D, Vinches , Henry J-P, Leveau Ph, Goutouli M, Thernot R. The building of the Roman aqueducts: Financial and technological problems. The case of the Arles aqueduct. In: Jansen G, editor. Cura Aquarum in Sicilia, Proceeding of the tenth international congress on the history of water management and hydraulic engineering in the Mediterranean region. 2000. p. 125–32.
[17] Finker M. Analyse comparée des amphithéâtres d'Arles et de Nîmes. Ph.D. thesis. Université Aix-en-Provence, France; 1988.
[18] Chetouane B. Approche combinée éléments finis/éléments discrets pour la modélisation des structures maçonnées. Ph.D. thesis. Université Montpellier II, France; 2004.
[19] Godefroy P, Lambert J, Levret A, Vaskou P. The French macroseismic database "SIRENE". In: 22nd general assembly of the European seismological commission. 1990.
[20] BRGM, EDF/TEGC, GEO-TER, IPSN/BERSSN. Université de Paris Sud. Paléosismicité et aléa sismique: Methodes d'études et recherches actuelles en France. Géochronique 1993; 46: 17–21.
[21] Ghafiri A. Paléosismicité des failles actives en contexte de sismicité modérée: Application à l'évaluation de l'aléa sismique dans le Sud-Est de la France. Ph.D. thesis. Univ. Paris-Sud, France; 1995.
[22] Granier Th, Grellet B, Carbon D, Combes Ph, Cushing M. Paleoseismicity studies in France: Main results. In: Fifth international conference on seismic zonation, AFPS-EERI, proceedings volume II. Ouest éditions Presses Académiques; 1995. p. 1562–9.
[23] DeMets C, Argus RG, Stein S. Current plate motions. Geophys J Int 1990;101: 425–78.
[24] ISMN. Zanjiran earthquake, Iran, June 20th 1994. http://www.bhrc.ac.ir/ISMN/SHABAKEH/accelerograms/earthquake/ten_years/zanjiran/zanjiran.htm.
[25] Cundall PA. A computer model for simulating progressive large scale movements of blocky rock systems. In: Proceedings of the symposium of the international society of rock mechanics, Vol. 1. 1971. p. 132–50.
[26] Cundall PA, Strack ODL. A discrete numerical model for granular assemblies. Geotechnique 1979;29:47–65.
[27] Acary V, Blaise JY, Drap P, Florenzano M, Garrec S, Jean M. et al. NSCD method applied to mechanical simulation of masonry in historical buildings using MOMA. In: XVII CIPA (international committee for architectural photogrammetry) international symposium WG3 - simple methods for architectural photogrammetry. 1999.
[28] Moreau JJ. Numerical aspects of sweeping process. Comput Methods Appl Mech Engrg 1999;177:329–49.
[29] Moreau JJ. Some numerical methods in multibody dynamics: Application to granular materials. J Mech A Solids 1994;13(Suppl. 4):93–114.
[30] Moreau JJ. Unilateral contact and dry friction in finite freedom dynamics. In: Moreau J, Panagiotopoulos P-D, editors. Non smooth mechanics and applications in CISM courses and lectures. Wien, New York: Springer-Verlag; 1988.
[31] Moreau JJ. Contact et frottement en dynamique des systèmes de corps rigides. Revue Européenne des Eléments Finis 2000;9:9–28.
[32] Moreau JJ. An introduction to unilateral dynamics. In: Frémond M, Maceri F, editors. Novel approaches in civil engineering. Springer Verlag; 2003.
[33] Jean M. The non-smooth contact dynamics method. Comput Methods Appl Mech Eng 1999;177:235–57.
[34] Jean M. Frictional contact in collections of rigid and deformable bodies: Numerical simulation of geomaterials. Amsterdam: Elsevier Science; 1995.
[35] Jean M, Moreau JJ. Unilaterality and dry friction in the dynamics of rigid bodies collection. In: Contact mechanics international symposium. Lausanne, Switzerland: Presses Polytechniques et Universitaires; 1992.
[36] Renouf M, Acary V, Dumont G. 3D Frictional contact and impact multibody dynamics: A comparison of algorithms suitable for real-time applications. In: Goicolea JM, Cuadrado J, Garcia Orden JC, editors. Multibody dynamics 2005, ECCOMAS thematic conference. 2005.
[37] Renouf M, Dubois F, Alart P. A parallel version of the non smooth contact dynamics algorithm applied to the simulation of granular media. J Comput Appl Math 2004b;168:375–80.
[38] Renouf M, Dubois F, Alart P. Numerical investigations of fault propagation and forced-fold using a non smooth discrete element method. Rev Euro Method Num 2006a;15:549–70.
[39] Dubois F, Jean M. LMGC90 une plateforme de développement dédiée à la modélisation des problèmes d'interaction. In: Actes du sixième colloque national en calcul des structures. CSMA-AFM-LMS; 2003.